Materials and Design 186 (2020) 108210

Contents lists available at ScienceDirect

Materials and Design

journal homepage: www.elsevier.com/locate/matdes

Rubbery nanofibers by co-electrospinning of almost immiscible NBR and PCL blends

Emanuele Maccaferri [a], Laura Mazzocchetti [a,b,*], Tiziana Benelli [a,b], Tommaso Maria Brugo [c,b], Andrea Zucchelli [c,b,*], Loris Giorgini [a,b]

[a] Department of Industrial Chemistry "Toso Montanari", University of Bologna, Viale Risorgimento 4, 40136 Bologna, Italy
[b] Interdepartmental Center for Industrial Research on Advanced Applications in Mechanical Engineering and Materials Technology, CIRI-MAM, University of Bologna, Viale Risorgimento 2, 40136 Bologna, Italy
[c] Department of Industrial Engineering, University of Bologna, Viale Risorgimento 2, 40136 Bologna, Italy

HIGHLIGHTS

- Production of long-time stable (at least 2 years) rubbery nanofibers without additional crosslinking required
- Homogeneous low T_g PCL/NBR blend with wide span of compositions (up to 80%wt NBR)
- Nanofibers with PCL-like crystal phase seemingly promoted by NBR/PCL interaction at molecular scale
- Improvements in mechanical performance with respect to plain PCL nanofibers
- Results interpreted with a phenomenological model, whose parameters take into account nanofibers composition and morphology

GRAPHICAL ABSTRACT

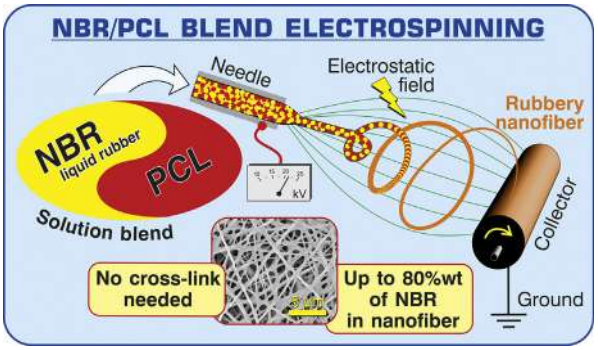

ARTICLE INFO

Article history:
Received 31 July 2019
Received in revised form 10 September 2019
Accepted 11 September 2019
Available online 13 September 2019

Keywords:
Nitrile butadiene rubber
Polycaprolactone
Electrospinning
Rubber nanofiber
Thermal properties
Tensile test

ABSTRACT

The paper presents a simple method for producing rubbery nanofibers without additional crosslinking required. Electrospinning's fast solvent evaporation is able to induce in liquid NBR/PCL pairs thermoplastic elastomeric (TPE) structure that holds stable over time without any further processing. The slight relative solubility of the polymers pair promotes a homogeneous blend formation with low T_g regions of blended NBR/PCL, avoiding phase separation. Such nanofibers show also a PCL-like crystal phase that is surprisingly higher than plain PCL nanofibrous counterpart and seemingly promoted by NBR/PCL interaction at molecular scale. The obtained nanofibrous-TPE morphology is reproducible, stable with time up to at least two years and is detected in a wide range of blend compositions (up to 80%wt NBR). Such a morphology reflects in good mechanical properties, which are analysed with a fitting model taking into account nanofibrous structure. Its impressive fitting ability helps interpretation of tensile tests behavior, carried out via normalization of force data with respect to sample mass, highlighting the contribution of liquid rubber in improving both elastic modulus and properties at failure. Such rubbery nanofibers represent a cost-effective powerful tool for the production of advanced self-damping composite materials with improved overall mechanical properties.

Data availability:

* Corresponding authors at: Interdepartmental Center for Industrial Research on Advanced Applications in Mechanical Engineering and Materials Technology, CIRI-MAM, University of Bologna, Viale Risorgimento 2, 40136 Bologna, Italy.
E-mail addresses: laura.mazzocchetti@unibo.it (L. Mazzocchetti), a.zucchelli@unibo.it (A. Zucchelli).

https://doi.org/10.1016/j.matdes.2019.108210

The raw and processed data required to reproduce these findings cannot be shared at this time as the data also forms part of an ongoing study.

1. Introduction

Nanofibers represent a powerful tool to design advanced structural and functional materials [1], and it is growing more and more the number of their applications, such as in biomedical devices, filtration media, wearable devices and electronics [2–5]. Besides, the use of nanofibrous membranes has been recognized as an efficient route to modify epoxy resin, where they act both as resin toughening agents, as well as bridging threads that keep the diverging edges together [6]. With this approach, improvements as high as two to three times the original reference values were observed in the energy release rate at initiation (G_C) and propagation (G_R) for delamination (either mode I or II), and in the fracture toughness of the material (K) [6]. Moreover, nanofibers can impart a lot of different functional properties [7], depending on their composition and properties, and they appear as a smart approach to locally modify the resin where required, as in the case of flame retardancy, without affecting the whole bulk material [8]. However, in all the reported studies, thermoplastic polymers are used, while the elastomeric counterpart might represent a smarter approach. Indeed, while rubber in the form of (nano)particles is among the most renown commercial toughening agents for composites, rubbery nanofibers are still not. Toughening is a requirement for brittle materials and can be attained by addition of already cross-linked rubbery particles, core-shell particles with rubbery core and glassy shell for easiness of handling, or liquid rubber homogeneously mixed to the polymers [9,10]. Within this frame, the possibility of manufacturing rubbery nanofibers to be used as toughener for, as an example, local modification of epoxy resin systems, in particular in composite materials, appears as an optimal combination of the two previously introduced toughening approaches.

Electrospinning represents the easiest way to attain nanofibrous morphology, but, due to the strict technological requirements of this process, the possibility of manufacturing elastomeric nanofibers is still an open issue, owing to the inability to process already crosslinked rubbers and to the complication of processing rubber precursors. In fact, the liquid rubber, which is not crosslinked, cannot be easily handled on its own due to the viscous behaviour of the polymer at room temperature [11], that, without cross-linking, prevents it from keeping a given shape for an indefinite amount of time [12–14].

Attempts at obtaining rubbery nanofibers are scarcely reported in the literature. In some cases, papers report just the proof of concepts of the possibility to electrospin rubber polymer solutions [15–17], or they attain (micro)fibers rather than nanofibers, with diameters in the micrometre range [18,19]. In most cases, however, the use of a curing agent in the formulation to cross-link the polymer is mandatory for avoiding nanofiber coalescence. The rubber cold flow phenomenon may be so relevant that the curing step has to be applied during electrospinning [12,13] or, at the latest, straightforwardly after the process [18–20], within a tightly limited time-span, down to a few minutes [14], that strongly limits the execution of the electrospinning process for prolonged time and, in turn, the final membrane thickness attained [14]. Other attempts involve more complicated procedures. Nie et al. coated nanofibers in gelatin before curing to avoid coalescence [21]. Although the process brings nanofibrous membranes with good mechanical properties, it appears tricky and multistep. Kim and Kim describe the possibility of producing fully Epoxidized Natural Rubber (ENR) fibers, but they obtain microfibers and, possibly owing to the poor handling of the material, they have to electrospin it directly onto a crude resin bed [22]. Finally, a method has been reported for rubbery nanofiber production, where the ENR is blended in a variable range with polyvinylchloride [23]. While nanofibers are reported to form, their characterization is poor, and no mechanical behaviour is discussed. Nitrile rubber has been blended with epoxy resin and electrospun to produce highly stretchable electrodes, but the crosslinking step is still required to maintain the nanofibrous morphology [20].

In this context, the blending approach to produce stable fibers could be a premiant idea. However, polymers are well renown to commonly phase separate owing to adverse thermodynamics when mixed together, thus limiting the number of fully miscible polymer pairs [24]. Nonetheless, blending is a simple and effective way to favourably combine attractive properties of different polymers in a single material, thus overcoming limitations and drawbacks associated with the single component. Miscible polymer blends can be easily recognized, since they form a single phase, characterized by single glass transition temperature (T_g) and a behaviour that lies in between the two pure polymeric extremes, and that also depends on the actual mixture composition, thus allowing a fine tailoring of the blend properties simply based on formulation [25]. While compatibilizers are often used to attain the miscibility even in the adverse cases, thermodynamics is able to guide in the choice of polymer pairs with ability to spontaneously blend together. Hence, with the aim of producing suitable composite modifiers, an assessment of the thermodynamic and kinetic possibility to blend together a polymer pair has been carried out to produce nanofibers: this is a simple and versatile method for the production of electrospun nanofibers without tricky processing steps [24,26].

Upon evaluation of the thermodynamic and the processing peculiarities, the production of nanofibrous membranes containing up to 80%wt of linear (non-cross-linked) carboxylated Nitrile Butadiene Rubber (NBR), commonly named Nipol, is presented. Such carboxylated rubber precursor was chosen for its renowned compatibility with epoxy resins, for the modification of whom this work is finally intended. In particular, the ability of the electrospinning process is demonstrated for providing a miscible blend of NBR liquid rubber with poly(ε-caprolactone) (PCL), which cannot be obtained with traditional techniques such as solvent casting and spin coating (Fig. 1). The obtained nanofibers are analysed in terms of miscibility range span and consequent thermomechanical properties and results are compared to mixture processed with different approaches, such as solvent casting and spin coating. Finally, mechanical properties of such membranes are measured, and their performances are analysed with the help of an innovative method put forward by the Authors. The obtained results demonstrate that, via electrospinning of liquid rubber with PCL, it is possible to attain the formation of a TPE-like structure that not only keeps together the fibers without the need for a chemical crosslinking, but it also provides excellent mechanical properties to the membrane without the need of additional treatment.

2. Materials and methods

2.1. Materials

Carboxylated nitrile butadiene rubber (NBR) NIPOL 1072CGX was purchased from Zeon Chemicals [68%mol butadiene (Bu), 28%mol acrylonitrile (ACN), 4%mol methacrylic acid (MAA)]. Poly(ε-caprolactone) (PCL), M_w 70,000-90,000, was purchased from Sigma-Aldrich. Polymers were both used without any preliminary treatment. *N*,*N*-dimethylacetamide (DMAc), *N*,*N*-dimethylformamide (DMF), formic acid and chloroform ($CHCl_3$) were purchased from Sigma-Aldrich and used without further purifications.

Please cite this article as: E. Maccaferri, L. Mazzocchetti, T. Benelli, et al., Rubbery nanofibers by co-electrospinning of almost immiscible NBR and PCL blends, Materials and Design, https://doi.org/10.1016/j.matdes.2019.108210

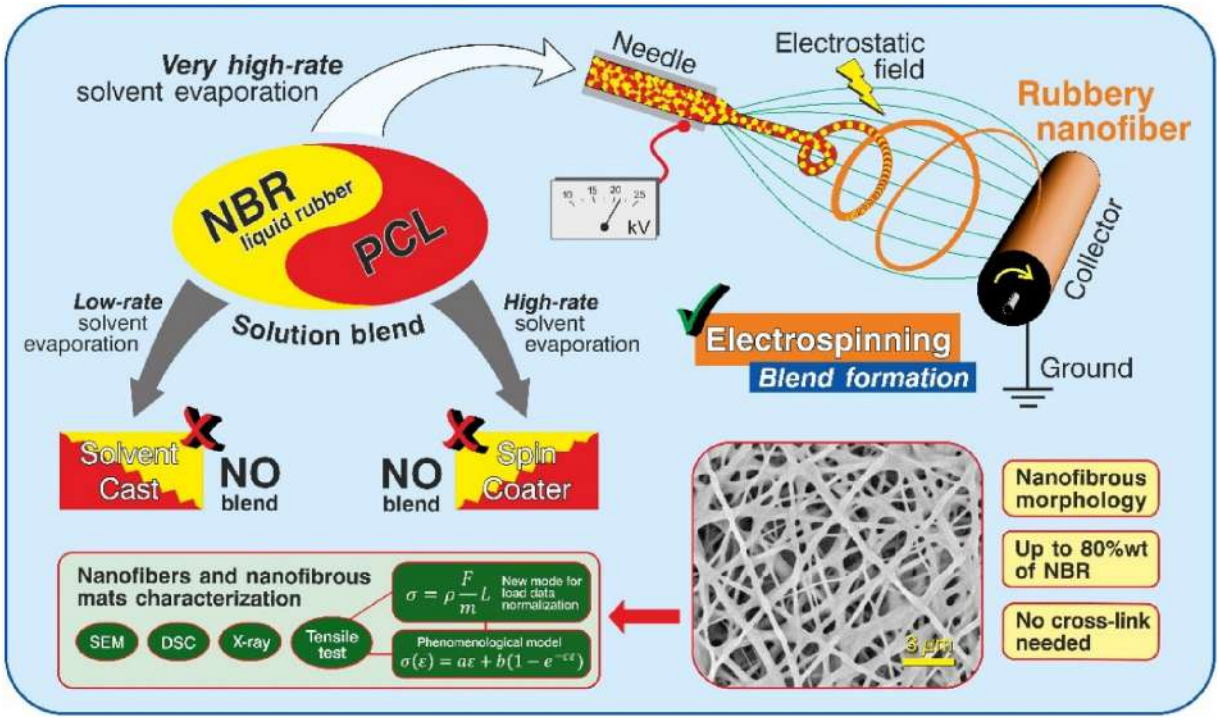

Fig. 1. Sketch of the paper rationale: electrospinning technique is applied as the only method to obtain homogeneous blend of a crystallizable polymer (PCL) and a liquid rubber (NBR).

2.2. Polymer solutions and blend preparation, viscosity measurements

NBR solution (S-NBR, 10%wt) was prepared in DMAc (e.g. 1.0 g of polymer in 9.6 mL of solvent) under magnetic stirring at room temperature until formation of homogeneous solutions.

PCL solution (S-PCL, 10%wt) was prepared in $CHCl_3$/DMF 1:1wt (e.g. 1.0 g of polymer in 3.0 mL of $CHCl_3$ and 4.8 mL of DMF) under magnetic stirring at room temperature until formation of homogeneous solutions.

NBR/PCL blends were prepared by mixing together S-NBR and S-PCL solutions in different proportions (20, 40, 60, and 80%wt of S-NBR solution), according to Table S1. Polymer blends were stirred for minimum 2 h to ensure proper homogenization.

Viscosity measurements were performed at 25 °C via rotational viscometer (Haake Viscotester 7 plus), equipped with R5 spindle at 200 rpm (except for the S-NBR and S-80/20, where R4 spindle was used to better comply the recommended viscosity ranges), using an adequate volume of solution.

2.3. Solvent casting and spin coating films production

Films obtained via solvent casting were produced pouring an adequate amount of polymeric solution/blend into a Petri dish which is kept for 18 h in environmental conditions and finally moved in a desiccator under vacuum for 6 h (3 dynamical + 3 static vacuum) to ensure complete solvent removal.

Films obtained via spin coating (Delta 20 BM, B.L.E. Laboratory Equipment GmbH) were produced placing a few drops of solution on a 20 × 20 mm microscope slide and applying the following program: 60 s at 2500 rpm, followed by 90 s at 3500 rpm (acceleration/deceleration ramps of 20 s). Samples were finally moved in a desiccator under vacuum for 6 h (3 dynamical + 3 static vacuum) to ensure complete solvent removal.

2.4. Nanofibrous mats production

Nanofibrous mats were produced using a Spinbow® electrospinning machine equipped with four 5 mL syringes. Needles (length 55 mm, internal diameter 0.84 mm) were joined to syringes via teflon tubing. Nanofibers were collected on a rotating drum covered with poly(ethylene)-coated paper at 50 rpm (tangential speed 0.39 m/s). Mats have final dimensions of approximately 30 × 40 cm. In Table 1 electrospinning process and environmental parameters for mats production are reported.

Table 1
Electrospinning process parameters and nanofiber diameters of produced nanofibrous mats.

Nanofibrous mat	Electrospun solution/Blend	Flow rate	Electric potential	Distance	Electric field [a]	Temperature	Relative humidity	Nanofiber diameter [b]
		mL/h	kV	cm	kV/cm	°C	%	nm
N-PCL	S-PCL	0.75	14.4	15.0	1.0	25–27	29–32	434 ± 196
N-20/80	S-20/80	0.70	17.0	13.0	1.3	22–25	23–25	238 ± 90
N-40/60	S-40/60	0.70	17.0	13.0	1.3	24–26	19–21	223 ± 56
N-60/40	S-60/40	0.55	18.3	13.0	1.4	22–24	20–22	253 ± 78
N-80/20	S-80/20	0.60	18.5	13.0	1.4	24–26	25–27	n.d.

n.d. = not detectable.
The electrospinning process was carried out until an adequate thickness of mat (ranging from 40 to 60 μm) was obtained.
[a] Calculated as electric potential to distance ratio.
[b] "As spun" nanofiber.

Please cite this article as: E. Maccaferri, L. Mazzocchetti, T. Benelli, et al., Rubbery nanofibers by co-electrospinning of almost immiscible NBR and PCL blends, Materials and Design, https://doi.org/10.1016/j.matdes.2019.108210

2.5. Characterization of nanofibrous membranes

Nanofibrous mats were analysed by Optical Microscopy with a Zeiss Axioscop and by scanning electron microscopy (SEM, Phenom ProX) to determine nanofibers morphology. All analysed surfaces were gold coated in order to make them conductive. The distribution of fibers diameters on the electrospun mat was determined via manual measurement of >100 single fibers by means of an acquisition and image analysis software (ImagePro Plus). Thermogravimetric (TGA) measurements were carried out using a TA Instrument SDT Q600 on 10 mg samples heating from Room Temperature (RT) up to 600 °C at 10 °C/min heating rate samples under inert atmosphere (nitrogen flow rate 100 mL/min), with a subsequent 30 min isotherm under oxidizing atmosphere (air flow rate 100 mL/min). Differential scanning calorimetry (DSC) measurements were carried out on a TA Instruments Q2000 DSC modulated apparatus equipped with RCS cooling system. In dynamic runs every sample (5 mg) was heated from 0 °C to 200 °C twice at 20 °C/min in nitrogen atmosphere, with an intermediate quench cooling. Wide-angle X-ray scattering (WAXS) were carried out at RT with a PANalytical X'Pert PRO diffractometer equipped with an X'Celerator detector (for ultrafast data collection). A Cu anode was used as X-ray source (K radiation: $\lambda = 0.15418$ nm, 40 kV, 40 mA), and 1/4° divergence slit was used to collect the data in 2θ range from 2° to 60°. Tensile tests of selected nanofibrous mats were made using a Remet TC-10 tensile testing machine equipped with a 100 N load cell, speed test 10 mm/min. Nanofibrous membranes were anchored in a paper frame, previously reported [27] (47 × 67 and 25 × 45 mm outer and inner dimensions, respectively), pasted with cyanoacrylate glue for better handling. Moreover, it guaranteed that all non-woven nanofibers were clamped in the machine fixtures. Effective specimen dimensions were 20 × 45 mm, (width) × (initial length), respectively. Paper frame was cut before the test started. After tensile test, the specimen was recovered and weighted for the stress (σ) calculation according to Eq. (2) (see Results and discussion, sub-paragraph 3.5). At least five specimens were tested for each nanofibrous mat type. The elastic modulus, maximum stress and elongation at break were evaluated. Tensile test data were analysed by means of a fitting model [27] which enable the direct evaluation of elastic moduli (Young modulus and the linear trend for high deformations) of the material (see Eq. (3), in Results and discussion, sub-paragraph 3.5).

3. Results and discussion

3.1. Electrospinning of plain NBR

The electrospinning technique, starting from polymeric solutions with conductivity and viscosity suitable for the process, is able to produce virtually continuous nanofibers with diameter well below the micron [28], resulting not only in high surface-to-volume ratio but also in a large aspect ratio. With the aim of electrospinning NBR, the non-crosslinked polymer has hence to be used. In the present case, a carboxylated NBR polymer containing 4%mol methacrylic acid (MAA) was investigated, the latter comonomer used for furthering miscibility with epoxy resins.

Preliminary solubility tests show the formation of rubber homogeneous solutions in acetone, amidic (DMF, DMAc) and chlorinated ($CHCl_3$, CH_2Cl_2) solvents. A first screening of the different solution possibility led to the choice of DMAc, owing to its well-known compatibility with the electrospinning process requirements [8], and a 10%wt solution of NBR in DMAc (S-NBR) was successfully electrospun (Fig. 2 A,

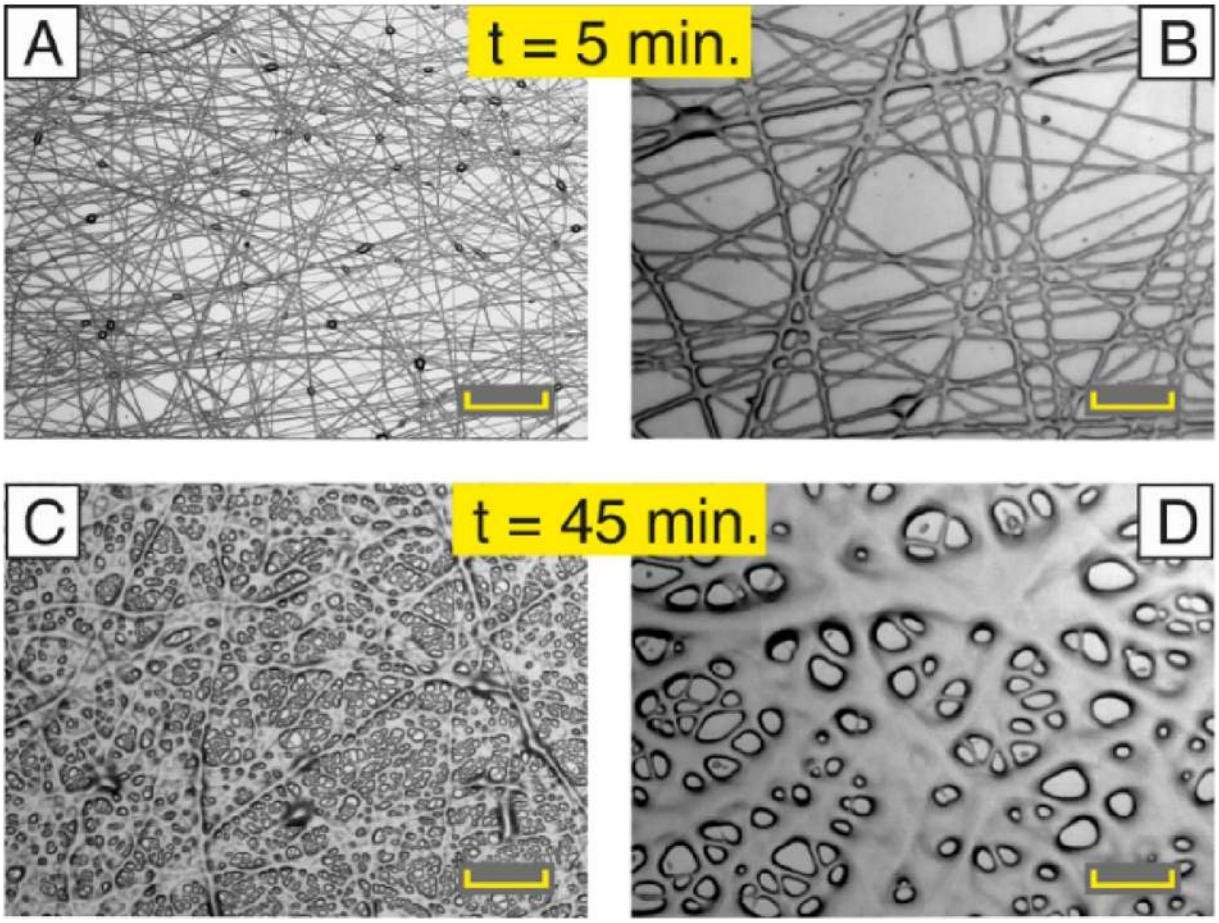

Fig. 2. Electrospun nanofibers from 10%wt NBR solution in DMAc (S-NBR). Nanofibers after 5 min (A, B) and after 45 min (C, D) of deposition. Scale bar: (A, C) 50 μm; (B, D) 10 μm.

Please cite this article as: E. Maccaferri, L. Mazzocchetti, T. Benelli, et al., Rubbery nanofibers by co-electrospinning of almost immiscible NBR and PCL blends, Materials and Design, https://doi.org/10.1016/j.matdes.2019.108210

B), with a fairly stable process. The obtained nanofibers, however, suffer significantly from dimensional instability, as already reported in the literature for similar systems [12–15], since individual fibers tend to coalesce one with the other, practically resulting in a film within a few minutes (Fig. 2 C,D). This process is displayed in Fig. 2 where optical microscope images of a pure NBR electrospun mat are shown as a function of time. Since this behaviour is due to the low glass transition temperature (Table 2) characterizing the elastomer precursor and the lack of crystal phases that help keeping the shape and mechanical properties, the same effect is prone to occur also for prolonged electrospinning deposition time, thus preventing the production of thick nanofibrous membranes as well as hampering the hypothesis of a later crosslinking of the NBR electrospun nanofibers at the end of their deposition.

3.2. Evaluation of NBR miscibility with PCL

With the aim of overcoming the poor handling properties of liquid rubbers and obtaining Room Temperature (RT) dimensionally and mechanically stable nanofibrous mats of rubbery materials which would not necessarily require a crosslinking stage during/after deposition, the possibility of blending the polymer with a compatible and miscible candidate has been investigated. The blending candidate should be able to provide nanofibers with good mechanical properties at RT and should be compatible with polymeric matrices (such as epoxies), leading to a positive interaction upon matrix processing. For example, Poly (ε-caprolactone) (PCL) proved to be a good epoxy toughener [6], with a crystal phase that, owing to the low melting temperature (T_m about 60 °C), disappears upon epoxy curing (which is usually carried out at least above 80 °C), leading to polymer dissolution within the epoxy matrix; moreover it has been already extensively studied the electrospinnability [6,30–34]. Assessment of PCL equilibrium miscibility with carboxylated NBR has been thus investigated via evaluation of the thermodynamic solubility parameter (δ) calculated for the polymer pair (see Supplementary Information paragraph SI1). A good miscibility occurs when the difference between the δ parameter for the polymer pair ($\overline{\Delta\delta}$,calculated according to Eq. S5 in the Supplementary Information) value is small, i.e. $\overline{\Delta\delta}$<5MPa$^{1/2}$, and partial miscibility could potentially be attained up to 10MPa$^{1/2}$ [26,35]. Based on the solubility parameter evaluation (see SI1), $\overline{\Delta\delta}$ for the NBR/PCL pair was found to be 7.9MPa$^{1/2}$, a value that does not account for an easy miscibility of the two components, tending instead toward an immiscible system. This behaviour should be critical and would not be expected to lead to the homogeneous and controlled material that is sought after for easy handling within composite reinforcement purposes stated in the introductory section. However, while the thermodynamics drives the intrinsic tendency of a polymeric pair to blend, sometimes kinetic factors affect the overall outcomes too. Within this frame, it has already been reported that the particular conditions of the electrospinning process, where a homogeneous solution jet is subjected to almost instantaneous evaporation of the solvent component, might be able to "freeze" partially miscible polymers in a single-phase material that would not separate afterwards [26].

In order to attain a homogeneous miscible blend via solubilization, the obvious prerequisite is to start from a homogenous solution of the two polymeric components. Hence a suitable solvent system has been sought after, that was able to comply with electrospinning processing requirements and could also represent a good starting point for the alternative wet processes (spin coating and solvent casting). While the DMAc previously used for NBR electrospinning was tested, when used to dissolve PCL it did not succeeded in polymer solubilization, with only some swelling obtained. Hence, after few attempts, a 10%wt PCL solution in $CHCl_3$/DMF 1:1wt mixture (S-PCL) was successfully prepared and homogenously blended with S-NBR (in DMAc, previously discussed). Several polymer ratios were used (see Table 2 for details) in order to evaluate whether a threshold polymer content would cause precipitation or separation of one of the many components of the complex mixtures: however, in no case such event was detected, and all the produced blend solutions are clear and do not display any evidence of phase separation phenomena while in the liquid phase. Hence starting from the different solution obtained (Table 2 and Table S1 in Supplementary Information for more detailed data), they were processed via solvent casting, spin coating and electrospinning, and the

Table 2
DSC data of nanofibrous mats, solvent cast and spin coater films, and the T_g prevision according to the Fox equation.

Sample	NBR	PCL	Experimental T_g I[a]	Experimental T_g II[a]	Expected T_g[b]	Melting temperature (peak)	Fusion enthalpy	Normalized fusion enthalpy[c]	PCL fraction crystallinity[d]
	%wt	%wt	°C	°C	°C	°C	J/g	J/g	%
PCL pellet	–	100	−58.4	–	–	64.0	76.5	76.5	54.8
NBR panel	100	–	−42.2	−13.7	–	–	–	–	–
N-PCL	0	100	−60.3	–	−60.3	60.9	68.7	68.7	49.2
N-20/80	20	80	−50.9	–	−52.4	65.8	63.7	79.6	57.1
N-40/60	40	60	−42.1	–	−44.0	61.0	52.4	87.4	62.7
N-60/40	60	40	−30.4	–	−34.8	60.9	35.5	88.6	63.5
N-80/20	80	20	−24.4	–	−25.0	56.4	19.8	99.1	71.0
N-NBR	100	0	−42.5	−14.2	−14.2	–	–	–	–
F-PCL	0	100	−59.8	–	−59.8	64.9	89.1	89.1	63.9
F-20/80	20	80	−46.6	n.d.	−52.1	64.7	67.8	84.8	60.8
F-40/60	40	60	−39.9	−14.2	−43.8	63.0	51.0	85.1	61.0
F-60/40	60	40	−40.8	−14.7	−34.8	63.6	40.0	100.0	71.7
F-80/20	80	20	−42.9	−17.7	−25.2	62.4	21.3	106.5	76.3
F-NBR	100	0	−42.8	−14.2	−14.7	–	–	–	–
SC-PCL	0	100	−57.0	–	−57.0	60.6	74.6	74.6	53.5
SC-20/80	20	80	−42.3	n.d.	−49.6	60.8	63.8	79.8	57.2
SC-40/60	40	60	−41.1	−12.4	−41.8	59.1	39.1	65.2	46.7
SC-60/40	60	40	−41.1	−14.8	−33.3	57.8	31.9	79.8	57.2
SC-80/20	80	20	−41.3	−18.8	−24.2	52.9	20.2	101.0	72.4
SC-NBR	100	0	−42.5	−14.2	−14.2	–	–	–	–

n.d. = not detectable.
[a] From DSC analysis.
[b] According to the Fox equation (Eq. (1))
[c] Referred to the PCL weight fraction.
[d] Considering the fusion enthalpy of 100% crystalline PCL equal to 139.5 J/g [29].

Please cite this article as: E. Maccaferri, L. Mazzocchetti, T. Benelli, et al., Rubbery nanofibers by co-electrospinning of almost immiscible NBR and PCL blends, Materials and Design, https://doi.org/10.1016/j.matdes.2019.108210

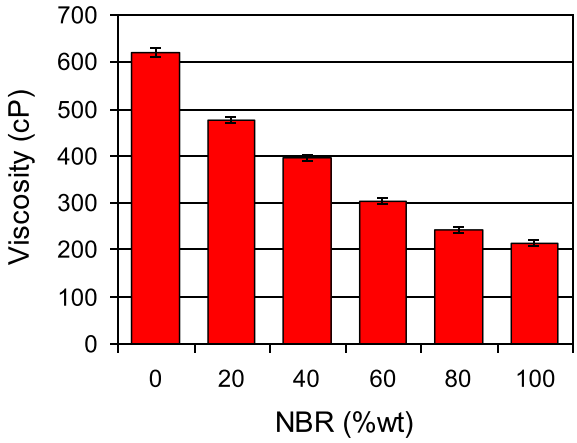

Fig. 3. Viscosity of PCL and NBR solutions, and of their blends.

results compared in terms of blending efficacy of the two thermodynamically poorly miscible polymers. It is worth to point out that the viscosity of the starting solutions is different and, as reported in Fig. 3, the blends behaviour lies more or less linearly in between the pure polymers.

3.3. Processing of NBR/PCL solutions

While the film morphology is not the most adequate for the composite modification purpose, nonetheless the investigation of the films that can be obtained from the homogeneous solutions produced (Table 2) might help getting some insights into the polymers blending ability. When the clear solutions are cast on a flat surface (Petri dish) and the solvent is allowed to evaporate at RT, discs with an average thickness of about 0.5–0.6 mm are obtained. Samples are labelled as F-X/Y, where X represents the NBR weight percentage and Y the PCL counterpart. For the sake of comparison, discs of the pure polymers, NBR and PCL, were also produced (and labelled as F-NBR and F-PCL), in order to check the effect of the processing conditions on the performance of these materials: in this case, pure NBR film appears sticky and inconsistent, thus not allowing its handling. All the obtained blended films appear opaque in the aspect, and white spots marring the surface appear and increase with increasing the PCL content with respect to the plain NBR that is an almost transparent compact film. All the blend cast films' consistency and aspect (Fig. 4) suggest that some crystallization occurred in almost all the samples, though its development is not homogeneously distributed in the bulk; moreover, F-60/40 and F-80/20 are sticky and difficult to handle as already reported for F-NBR.

Since the two polymers are expected to hardly blend, and the kinetic aspect of the processing might thus play an important role in the ability to keep together NBR and PCL, an attempt at forming miscible blends via spin coating of the prepared homogenous solutions was also carried out, in order to assess the effect of the rapid solvent evaporation of this processing technique in comparison with the slow solvent evaporation at RT. Thin membranes were obtained, whose aspect appears definitely more homogeneous than cast films and they were labelled SC-X/Y, where once again X represents the NBR weight percentage and Y the PCL counterpart.

The very same solutions already used for solvent casting films, were also electrospun. All the different formulations were able to successfully lead to nanofibers once process parameters' optimization has been blandly tailored on the specific solution characteristics (Table 1), thus providing in each case a stable process, with neither drops expulsion nor needle obstruction. Nanofibrous mats, labelled as N-X/Y, do not show evidence of macroscopic defects, such as holes or sputtered material. While a wide range of different solution compositions has been investigated with the aim of finding the tentative threshold PCL content required to attain nanofibrous morphology, surprisingly the fibrous morphology is detected for all the produced samples, though at high NBR fractions some filming also occurs.

Such a behaviour is clearly displayed in Fig. 5, where SEM micrographs of the different electrospun mixtures are shown at different magnifications, together with plain PCL nanofibers (N-PCL) for the sake of comparison (N-NBR is displayed in Fig. 2): it is worth pointing out that all the images were recorded at least 5 days after deposition, in order to emphasize the stability of the fibrous morphology. Additionally, micrographs taken after 24 months storage at RT still display the same unaltered morphology of the membranes (see Supplementary Information, Fig. S1). While the fibrous morphology is always obtained,

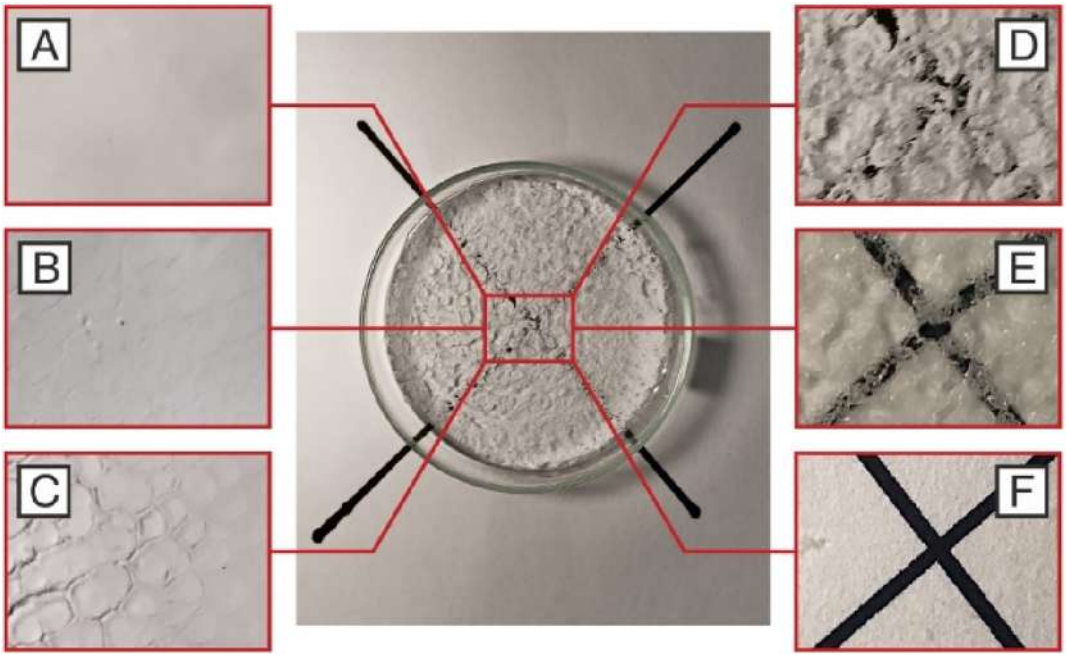

Fig. 4. Pictures of solvent cast films: A) F-PCL, B) F-20/80, C) F-40/60, D) F-60/40, E) F-80/20, F) F-NBR.

Please cite this article as: E. Maccaferri, L. Mazzocchetti, T. Benelli, et al., Rubbery nanofibers by co-electrospinning of almost immiscible NBR and PCL blends, Materials and Design, https://doi.org/10.1016/j.matdes.2019.108210

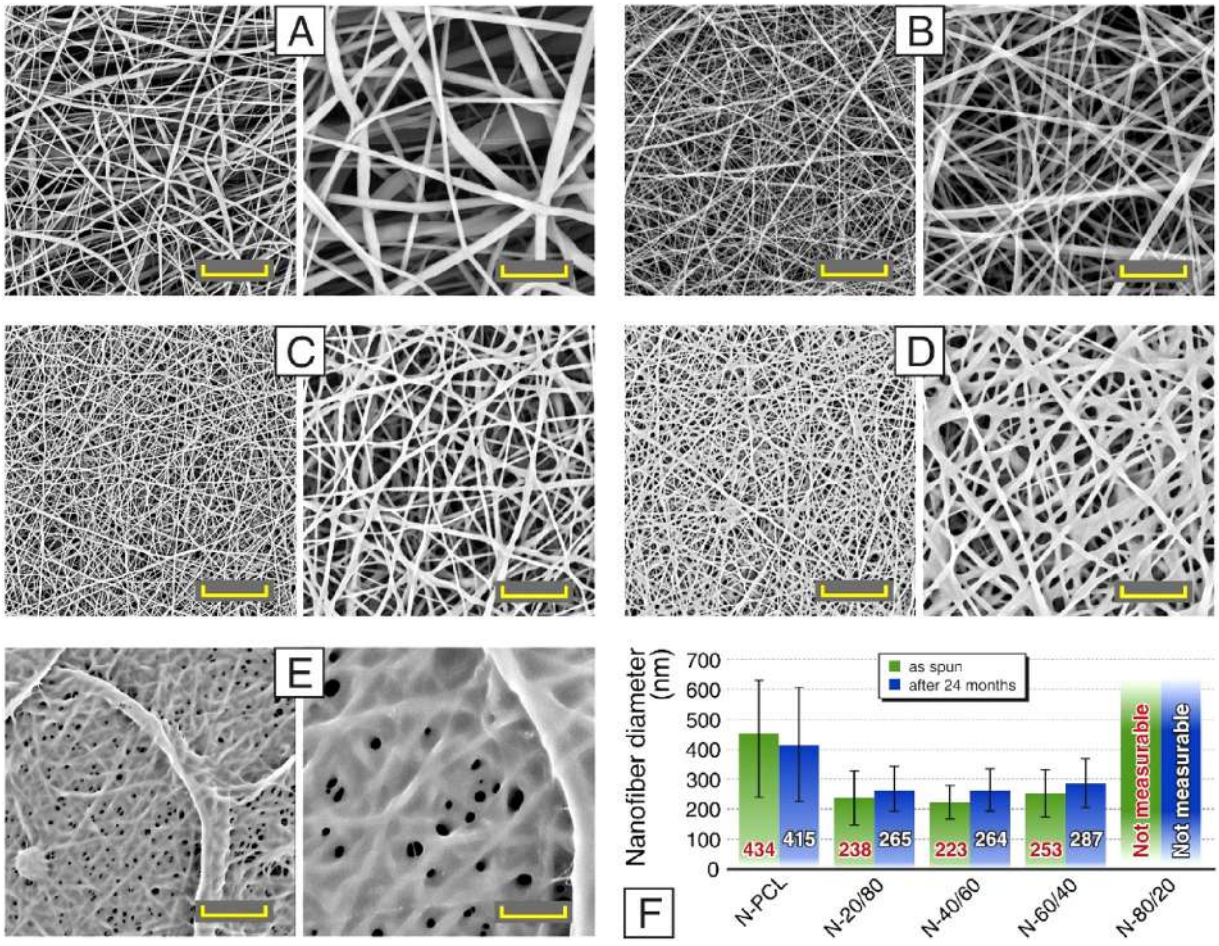

Fig. 5. SEM images of nanofibrous mats: A) N-PCL, B) N-20/80, C) N-40/60, D) N-60/40, E) N-80/20. Scale bar: left (5000×) 12 μm, right (15,000×) 4 μm. F) comparison of the average fiber diameters "as spun" and after 24 months.

increasing NBR content it can be clearly observed that fibers tend to join at the cross sections, and finally, when NBR represents 80% of the polymeric mass, there is a tendency to fill the cavities with some filming material (Fig. 5E). Nonetheless, it clearly appears that fibrous morphology is present and stable with time even in the most extreme formulations. The average diameter of nanofibers, evaluated via SEM micrograph analysis for all the samples with the exception of the N-80/20 due to the filming effect, stays well below the micrometre threshold in all cases (Fig. 5F). In particular, a sudden drop in the fibers diameter is observed going from pure N-PCL to the blends: this behavior can be attributed to both the different polymer/solvent system mixture used for every electrospun sample that, as depicted in Fig. 3, affects the final solutions viscosity, and to the application of a higher electrostatic field (1.3–1.4 vs 1.0 kV/cm) required for processing polymer mixtures with respect to plain PCL.

3.4. Thermal characterization of NBR/PCL films and nanofibrous membranes

All the obtained samples were subjected to thermal analysis for investigating the behaviour of the polymeric components upon processing, and as a function of the processing conditions. A preliminary TGA run (graph not shown) rules out the presence of residual solvent within both films and nanofibers, that could somehow affects thermal behaviour of the polymers in the further investigations. All prepared film samples were analysed by differential scanning calorimetry (DSC) and Table 2 collects their thermal characterization data together with results obtained for the plain polymeric components NBR and PCL, both in film (F-PCL and F-NBR) and pellet form, for the sake of comparison.

In the present case, as shown in Table 2, PCL thermogram displays two events, with a low temperature stepwise transition ascribed to the polymer glass transition centered at −58 °C (T_g), and an endothermic peak typical of crystal phase melting around 64 °C, whose entity increases upon solvent casting. It is indeed renown that solubilized crystalline polymers are strongly influenced by the solvent in their ability to crystallize [36] thus possibly promoting crystal formation in the cast PCL. Carboxylated NBR, instead, shows only a complex stepwise transition, that can be separated in two different events centered at −14 and −42 °C respectively. Such a behaviour has been already observed in poly(butadiene-*co*-acrylonitrile) copolymers [37] where, depending on the polymerization condition, poly(Bu-*alt*-ACN) rich segments form first, and finally poly(butadiene) homopolymer rich blocks add upon ACN depletion [38]. The addition of MAA comonomer does not alter this twofold situation, but tends to increase both T_gs with respect to literature data referred to plain NBR, possibly owing due to the intrinsic stiffness and H-bonding ability [39] of the methacrylic *co*-unit ($T_{g\ Poly(MAA)} = 300$ °C [40]).

When analysing NBR/PCL mixtures, it is expected that, in the case they are able to form a miscible polymer blend, they would display a single T_g, whose value should lie between the glass transition temperature of the individual reference polymers, given that the reference polymers have T_gs values at least 20 °C apart and represent at least 10%wt of the total mass [25]. Moreover, the blend glass transition temperature often exhibits a composition dependence that can be well described

Please cite this article as: E. Maccaferri, L. Mazzocchetti, T. Benelli, et al., Rubbery nanofibers by co-electrospinning of almost immiscible NBR and PCL blends, Materials and Design, https://doi.org/10.1016/j.matdes.2019.108210

by a mathematical equation, of which the most renown is the empirical Fox equation (Eq. (1))

$$\frac{1}{T_g} = \frac{w_1}{T_{g1}} + \frac{w_2}{T_{g2}} \quad (1)$$

where w_1 and w_2 are the weight fractions and T_{g1} and T_{g2} are the glass transition temperatures of Polymer 1 and 2 respectively, while T_g is the blend glass transition temperature (temperatures expressed in Kelvin).

The obtained solvent cast films are all characterized by the presence of both a stepwise transition and an endothermic peak (Table 2). All but F-20/80 samples display the same complex stepwise transition discussed for NBR, with double T_g, whose values are very similar to those of the plain NBR. F-20/80 shows instead a single step transition centered at an intermediate value between PCL and the lowest T_g in NBR, as plotted in Fig. 6A.

While it could be argued that there is the lack of PCL T_g in all the samples, nonetheless the trend displayed in Fig. 6A is clearly not typical of a blend, since no clear composition correlation is set. For the sake of comparison, the trend of the previously discussed Fox equation (Eq. (1)), is also sketched in Fig. 6A. In the present case the lack of PCL T_g could be tentatively ascribed to the presence of a significant crystal phase melting at a temperature that is compatible with that of the polyester (Table 2). WAXS analysis, carried out on all the solvent cast films and displayed in Fig. 7A, confirms indeed that the crystal phase can be attributed to the PCL, whose typical reflection can be observed in all the diffractograms [41–43], with an increasing broad amorphous halo that becomes more and more visible with increasing NBR fraction in the mixture. Such a condition would render the glass transition of the crystalline polymer (PCL) almost undetectable when the polymer fraction is around 20%wt, which actually corresponds to a mere 11%mol polyester.

Though the visual aspect of the spin coated specimens suggests a higher extent of homogeneity, the T_gs recorded for such samples perfectly match the trend previously discussed for the unblended films, as reported in Table 2 and displayed in Fig. 6B, showing that not even spin coating was able to provide miscibility. Analogously to the previous films (either cast or spin coated) investigation, electrospun membranes were analysed by DSC, and measurements were carried out on all the obtained nanofibrous samples, as well as on the reference nanofibrous PCL: the obtained data are summarized in Table 2. NBR/PCL nanofibrous mats all show one single glass transition temperature (T_g) below RT in the whole span of analysed compositions, ranging between the T_g of PCL and the higher value of the NBR glass transition temperature; above RT an endothermic event is detected. When plotted against the mixture composition, the position of the single T_g perfectly agrees with the values calculated on the basis of Fox Equation (Eq. (1)), whose trend (obtained using the higher value of $T_{g\,NBR}$) is also sketched in Fig. 6C for the sake of comparison. Such a behaviour, which is substantially different from the one observed for filmed and spin coated mixtures, seems to suggest the formation of a miscible blend [25]. It was indeed found, based on the Hansen solubility coefficient evaluation, that the two polymers are not completely immiscible and, as such, the ability to homogenously blend together and to form a single phase was not completely ruled out. Hence, in the case of the electrospinning process the extremely rapid solvent mixture evaporation occurring during the jet stretching within the electrostatic field might be responsible for freezing the homogenous polymeric solution in a single phase, that does not tend to separate afterwards, owing to some extent of thermodynamic interaction highlighted by the $\overline{\Delta\delta}$ value calculated above.

However, such a tendency is not sufficient to actively promote the blending of the polymers at the molecular level and keep them together when the solvent system slowly evaporates upon casting. When, indeed, the film is cast, the complex mixture of different solvents (DMAc, $CHCl_3$, DMF) will sequentially evaporate, creating an environment with different affinity for the two macromolecules that could contribute to their segregation owing to an overall poor tendency to blend together.

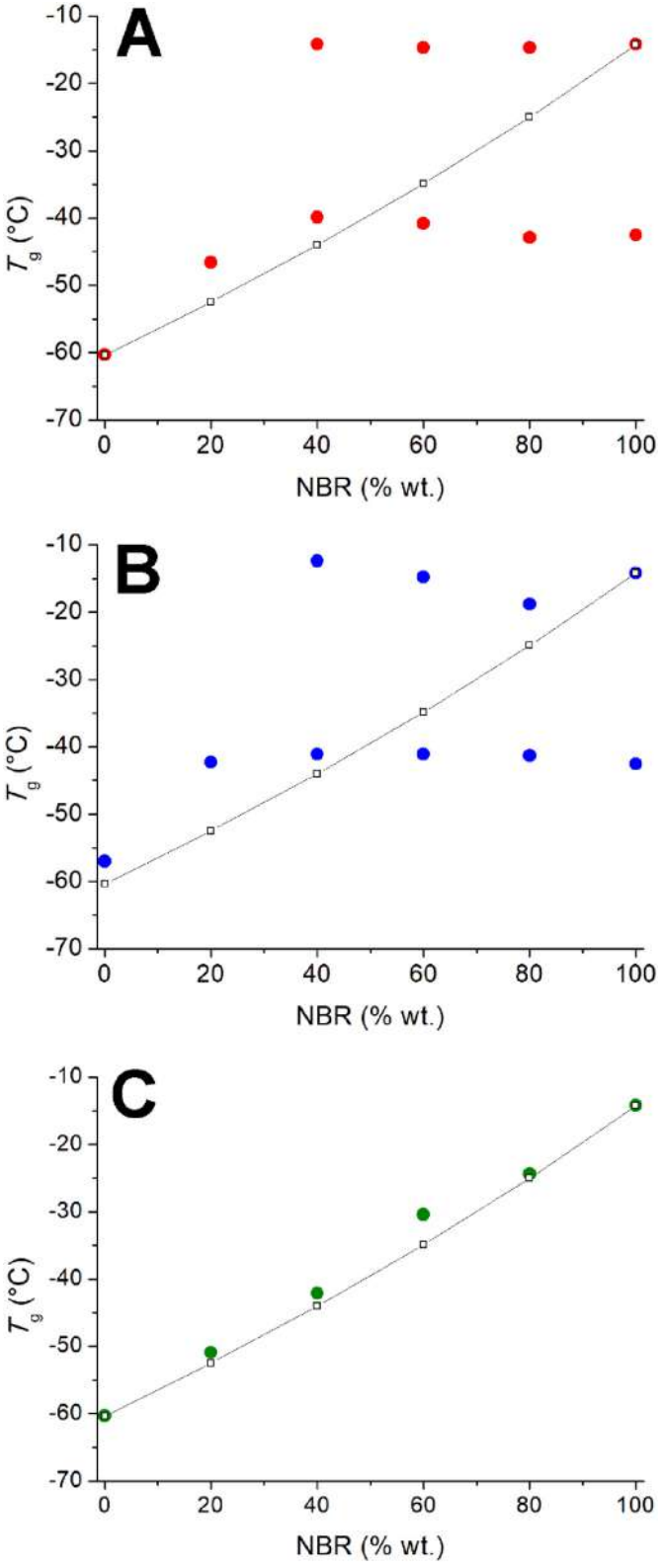

Fig. 6. Glass transition temperatures (T_g) as a function of NBR fraction (%wt) of A) solvent cast films, B) spin coating films and C) nanofibrous mats. Solid dots: T_g from DSC analyses; white squares: T_g calculated by Fox equation (Eq. (10).

The ability of the electrospinning to promote non-equilibrium miscibility of two partially miscible polymer has already been reported and demonstrated on a 50/50%wt mixtures [26]: however, to the best of

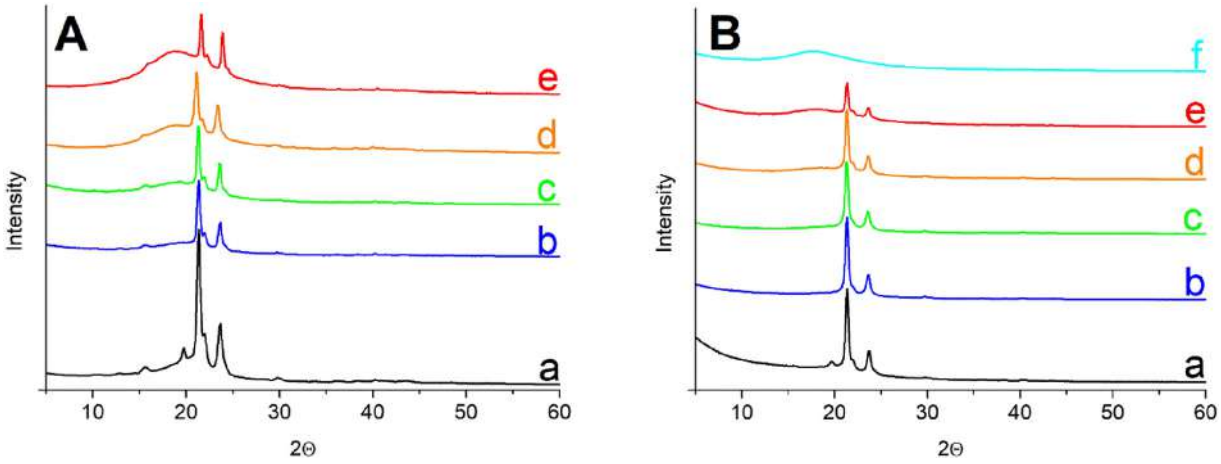

Fig. 7. WAXS diffractograms of (A) solvent cast films and (B) nanofibrous mats: a) PCL, b) 20/80, c) 40/60, d) 60/40, e) 80/20, f) NBR.

the Author's knowledge, the evaluation of a wide range of blend compositions obtained via electrospinning, such as the one presently discussed, has not yet been explored. Additionally, the analysed nanofibrous blends also display a prominent endotherm along the whole range of composition which can be associated to the presence of crystalline PCL domains.

Such an attribution is confirmed by the WAXS diffractograms reported in Fig. 7B, where the typical peaks appear at $2\Theta = 21.40°$ and 23.70°, corresponding to the (110) and (200) reflections from the orthorhombic unit cell of PCL [41–43].

It is worth pointing out that in the electrospun nanofibrous mats the (102) and (111) reflections substantially decrease, or even disappear, not only in the blends, but also in the plain PCL sample. In such systems, indeed, while the amorphous fraction of polymers is mixed at molecular level, a phase separated crystal region might form, rich in the crystallizable polymer. In these conditions the decrease in the chemical potential of the crystallizable polymer occurring upon addition of a diluent (a second polymer in the present case) will result in an equilibrium melting point decrease. An additional way to assess the miscibility of the system is, thus, the evaluation of melting point depression for crystalline/compatible polymer blends. The present system, however, does not display the smooth linear trend expected according to the equation drawn by Nishi and Wang [44] (see supplementary information SI2 for the evaluation of the melting point depression according to Nishi-Wang approach). The Nishi-Wang equation, however, has been drawn for equilibrium conditions, and melting points applied to verify the equation should be equilibrium values too. In the present case, though, this is not possible: the electrospinning processing conditions are far from equilibrium, and whatever treatment applied to the nanofibers to evaluate the equilibrium conditions values, such as isothermal crystallization and Hoffman-Weeks extrapolation [45], would remove the nanofibrous morphology thus altering the whole system. Hence the lack of correlation in the present data might strongly be affected by peculiar morphologies due to the processing conditions. In this context, the plot of melting enthalpies calculated for the different blend compositions, as well as for the plain electrospun and pristine PCL, versus the actual weight composition of the blend provides some interesting insight in the crystallization ability within nanofibers. The electrospinning is known to hamper the ability of a polymer to arrange in a crystal phase and the smaller the fiber diameter the higher the draw ratio, which tends too to hamper the formation of big and perfect crystals [27,33]. Accordingly, the electrospun PCL nanofibers display (Fig. 8) a lower crystal phase content with respect to the reference pristine polymer (ΔH_m decrease by about 10%, see Table 2).

The addition of a second component should further hamper, or at least leave unaffected, the crystallization ability of the polyester fraction in the blend. Surprisingly, the plot reported in Fig. 8 displays a perfectly linear trend of crystal fraction within the blends, whose extrapolation points to a crystal content in line (actually slightly higher) with the pellet PCL, leading also to a positive intercept at null PCL content (5.7 J/g). This behaviour is even more impressive when considering that, for example, 80%wt corresponds to 66%mol of PCL, and it seems to suggest that not only PCL is unaffected by the electrospinning in its ability to crystallize when homogeneously mixed with NBR, but the presence of the liquid rubber component has a nucleating effect that overcomes the hampering issues connected to the electrospinning processing: such an effect seems to increase with increasing the non-crystallizable polymer content. The presence of such a strong crystallizing ability, which is actually boosted by the presence of the co-component, is possibly the reason that makes nanofibrous membranes so manageable even at very high NBR content: while both polymers and their blends have indeed low T_g, the crystal phase promoted at impressively high fraction by the second component allows the system to keep the fibrous morphology without requiring any additional treatment (e.g. rubber cross-linking).

The structure hypothesized above for the nanofibers is actually reminiscent of a thermoplastic elastomer (TPE) [46,47] which comprises at least two interconnected polymer phases, one that is hard at RT but becomes fluid at high temperature (PCL crystal regions), while the other

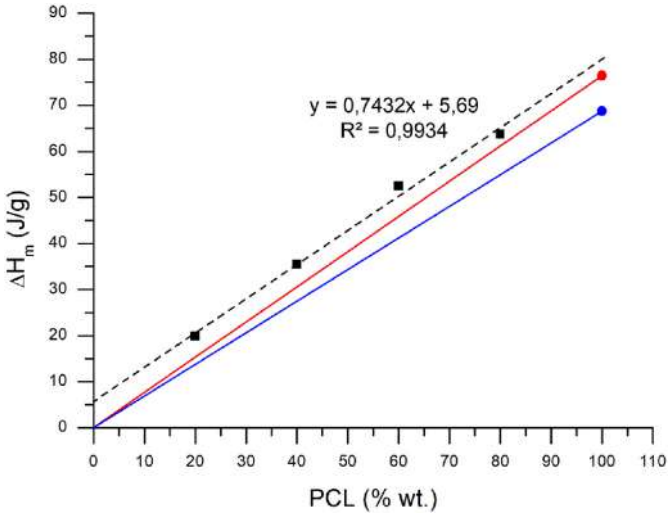

Fig. 8. PCL melting enthalpy (ΔH_m) of NBR/PCL nanofibrous mats (black squares), PCL pellet (red dot) and PCL nanofibers (N-PCL, blue dot). The red and blue lines represent the ΔH_m extrapolation of the enthalpy trend to 0% of PCL. The black dashed line is, instead, the linear regression line evaluated for NBR/PCL nanofibrous mats ΔH_m values, whose equation is also reported on the graph. (For interpretation of the references to colour in this figure legend, the reader is referred to the web version of this article.)

Please cite this article as: E. Maccaferri, L. Mazzocchetti, T. Benelli, et al., Rubbery nanofibers by co-electrospinning of almost immiscible NBR and PCL blends, Materials and Design, https://doi.org/10.1016/j.matdes.2019.108210

phase is soft and elastic in the same condition (PCL/NBR blended regions). Hence the electrospinning seems able to promote the straightforward formation of thermoplastic elastomeric nanofibers, which are stable at RT, thus bypassing many of the drawbacks that up to now hampered the production of non-crosslinked rubbery nanofibers.

3.5. Mechanical characterization of NBR/PCL nanofibrous membranes

All nanofibrous mats, except the N-80/20, were mechanically tested to evaluate their tensile behaviour. The N-80/20 sample was not tested due to the aspect of the fibers, that appeared partially filmed (Fig. 5E) and cannot be measured. For each type of selected material at least 5 specimens were tested.

Force-displacement results were analysed in terms of stress-strain curves, according to a recently reported procedure [27] where stress (σ) is calculated by means of Eq. 2 that describes σ as a function of simple and easy to measure quantities:

$$\sigma = \rho \frac{F}{m} L \tag{2}$$

where "ρ", expressed in mg/mm^3, is the material density (not the apparent membrane density), "m" is the specimen mass (in mg), "L" is the specimen initial length (in mm), F is the force (in N) and σ is the stress expressed in MPa. In the present case, ρ has been evaluated as the weighted average value of the two pure polymeric components density, according to nanofiber specific composition (Table S4 in Supplementary Information). In Fig. 9A the relative stress-strain curves are reported. The load normalization based on specimen mass instead of its dimension is useful for discarding any membrane thickness discrepancy due to the instrumentation used for its measurement, and to obtain more reliable tensile test results, thus unaffected by the membrane porosity.

It is worth mentioning that in all diagrams in Fig. 9A it is possible to distinguish three main stages in the material behaviour, as sketched in Fig. 9B: an initial nonlinear trend (Stage I), a subsequent linear trend (Stage II) at higher strain values, and finally a second nonlinear behaviour (Stage III), at which the stress and strain reach their maximum values before failure. Such a trend has been reported in several works discussing mechanical behaviour of nanofibrous samples [27,48–50].

The preliminary analysis of stress-strain curves was done considering Stage III and in particular the maximum values of stress (σ_{max}) and the related values of strain ($\varepsilon @ \sigma_{max}$) for the four investigated materials were determined (see Fig. 10).

Data displayed in Fig. 10 clearly show that, with respect to the pure PCL nanofibrous mat, there is an almost general tendency to increase both σ_{max} and $\varepsilon @ \sigma_{max}$. In particular, N-20/80 shows a significant increment of the mechanical performances of the nanofibrous mat, with the highest increase in terms of stress (+107%), whereas the increment in terms of strain at the maximum stress is limited (+27%). Then, the greater is the NBR fraction in the blend, the higher is $\varepsilon @ \sigma_{max}$, up to +154% in the case of 60%wt of NBR, while a decreasing trend for σ_{max} is observed with respect to the performance of N-20/80, down to a value that in N-40/60 is still significantly higher than pure PCL (+48%) while drops below the pristine polymer for N-60/40.

With the aim of providing a comprehensive picture of the overall nanofibrous mechanical behaviour, Stages I and II of the curves have to be analysed and interpreted and, in order to account for the nonlinear and linear segments of the curves, a mathematical model is thus put forward. The model described by Eq. (3) was previously reported and discussed [27] and it is based on the combination of two contributions, the first is a linear term and the second is a nonlinear exponential one:

$$\sigma(\varepsilon) = a\varepsilon + b - be^{-c\varepsilon} = a\varepsilon + b(1 - e^{-c\varepsilon}) \tag{3}$$

where "a", "b" and "c" are adimensional parameters experimentally determined to obtain the best data fitting using the least squares method.

It was thus possible to obtain an analytical expression for the material stiffness as in Eq. (4):

$$\frac{d\sigma}{d\varepsilon} = E(\varepsilon) = a + bce^{-c\varepsilon} \tag{4}$$

Eq. (4) allows to derive two parameters which can be used to study and characterize the material behavior:

1) the initial material stiffness (or initial Young's modulus, E_0)

$$E_0 = \lim_{\varepsilon \to 0} E(\varepsilon) = a + bc \tag{5}$$

2) the linear stiffness (or the Young's modulus of the linear trend of stress-strain curve, E_{lin})

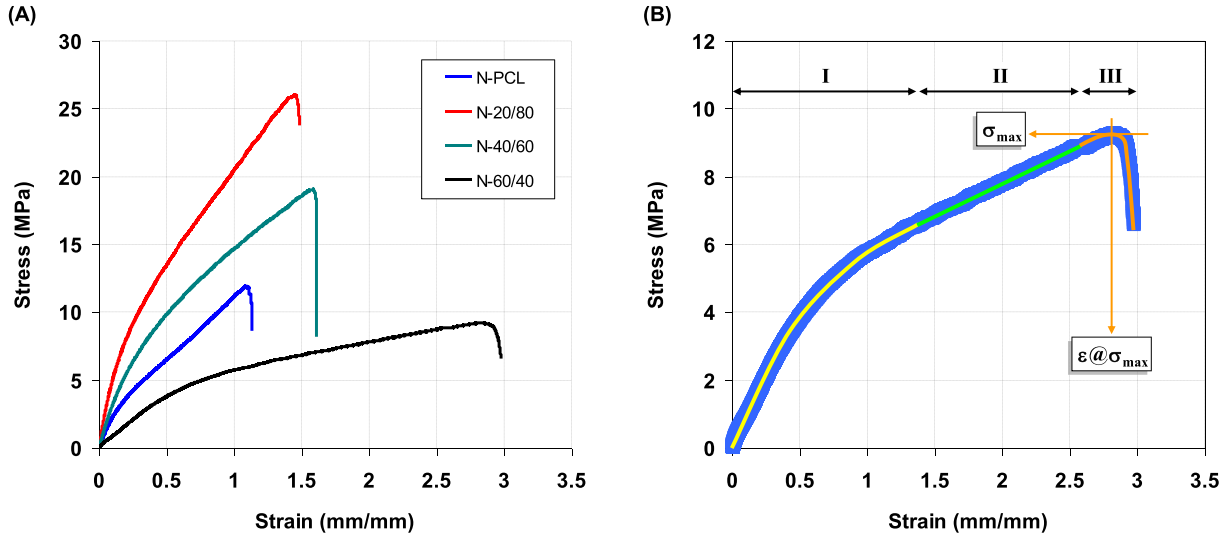

Fig. 9. A) Examples of stress-strain curves calculated according to Eq. (2). B) Identification of the three regions which characterize the mechanical behaviour of the material and the two parameters, maximum stress (σ_{max}) and its corresponding strain ($\varepsilon @ \sigma_{max}$), which characterize the final nonlinear trend of the curve (Stage III). Curves displayed in the figure were selected to best fit the average values calculated for each batch of specimens.

Please cite this article as: E. Maccaferri, L. Mazzocchetti, T. Benelli, et al., Rubbery nanofibers by co-electrospinning of almost immiscible NBR and PCL blends, Materials and Design, https://doi.org/10.1016/j.matdes.2019.108210

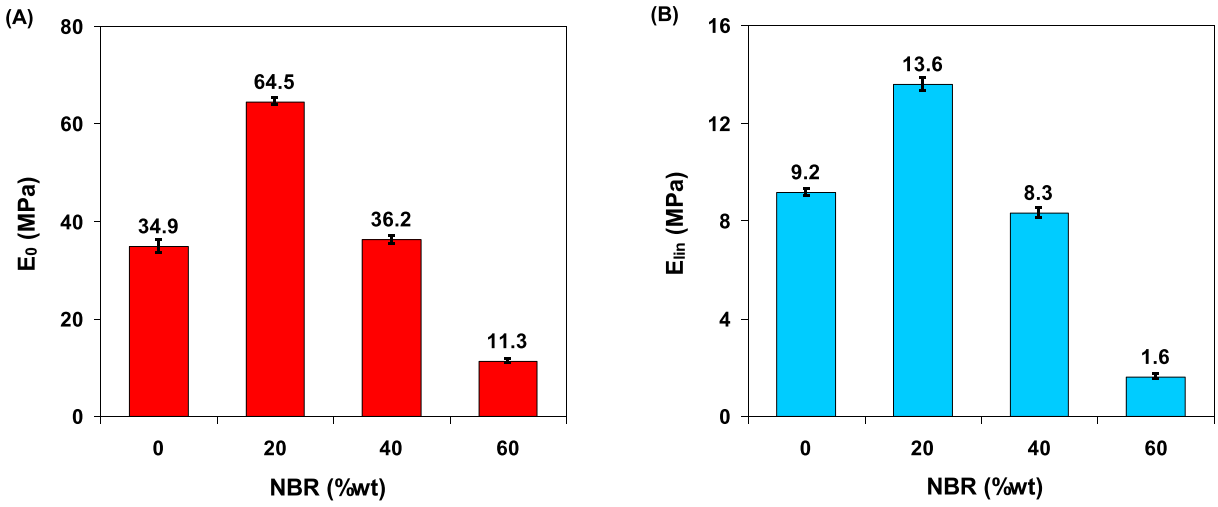

Fig. 10. A) Maximum values of stress (σ_{max}) and B) the corresponding strain (ε @ σ_{max}) for samples having different %wt content of NBR.

$$E_{lin} = \lim_{\varepsilon \to \infty} E(\varepsilon) = a \quad (6)$$

Application of such model to the presently investigated materials highlights an impressive fitting ability of the experimental data (see supplementary information SI3 for additional specifics of nanofibrous mats mechanical behavior) and it was thus possible to calculate the two main parameters, E_0 and E_{lin} (Fig. 11), for the set of previously discussed specimens.

When applying the proposed fitting model (Eq. (3)), the obtained results for the blend nanofibers clearly display that, starting from plain PCL, NBR addition to the nanofiber composition helps improving both the elastic modulus E_0 and the properties at failure (σ_{max} and ε @ σ_{max}). F-20/80 has unexpectedly high modulus and toughness (σ_{max} and ε @ σ_{max} both increase with respect to plain N-PCL), while F-40/60 has a modulus that almost matches the one of N-PCL, but with far higher properties at break. This effect could be attributed to both the excess of crystal phase and possibly also to some fiber weld joints induced by the presence of the liquid rubber in the system that is increasing in content. Such a behaviour, however, agrees with the previously discussion on the PCL degree of crystallinity (Table 2), that was found to be surprisingly high considering the presence of a significant amount of the second non-crystalizing component (NBR), and the processing via electrospinning that is renown to depress crystallization. Moreover, the overall behaviour agrees with the assumption that a TPE-like structure is formed upon electrospinning of the mixture and such a morphology not only keeps together the fibers without the need for a chemical crosslinking, but it also provides excellent mechanical properties to the membrane without the need of additional treatment (e.g. rubber cross-linking). Indeed, the elastic modulus (E_0) drops below the plain N-PCL value only at NBR content around 60% wt (F-60/40): while it could have been expected a strong plasticizing effect from NBR in all the range of compositions, this, in fact, only happens at very high liquid rubber fractions and with limited drawback on mechanical performance. F-60/40 still has impressing toughness and high properties at break, owing to the thermoplastic elastomeric morphology attained during the processing. The reasons underlying such a complex behaviour can be found both in the trend of the crystal phase content and in the nanofibrous mat architecture in terms of joints between fibers. While the latter parameters should increase in efficiency upon growing the fraction of NBR, the crystal phase, which is expected to decrease in the same conditions, has been found surprisingly high, thus justifying an unexpected positive performance of N-20/80 and to some minor extent of N-40/60 in terms of E_0. An additional parameter that has to be taken into account is the average diameter that, in the case of blends, is significantly smaller than N-PCL (about half of the N-PCL value, Fig. 5F), and such a morphological character has been proven to boost

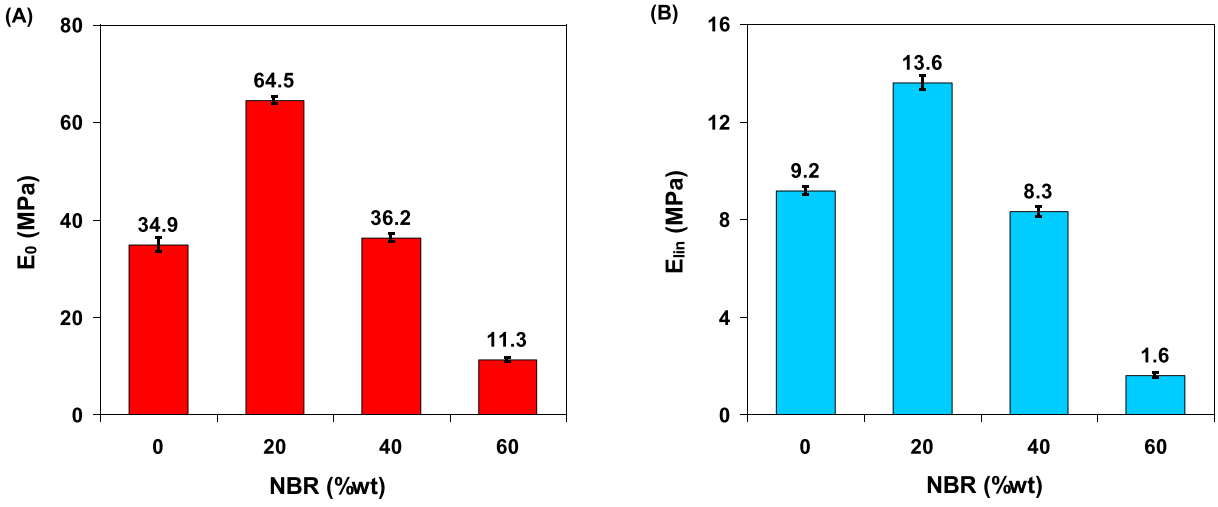

Fig. 11. Mechanical properties evaluated according to the model proposed in Eq. (3): A) initial material stiffness (E_0) and B) material stiffness in the linear trend (E_{lin}).

Please cite this article as: E. Maccaferri, L. Mazzocchetti, T. Benelli, et al., Rubbery nanofibers by co-electrospinning of almost immiscible NBR and PCL blends, Materials and Design, https://doi.org/10.1016/j.matdes.2019.108210

mechanical performances when it gets below a given threshold which might be peculiar to the polymeric system but has been reported to be in the order of 400–500 nm [51,52].

Non-woven mats deformation is driven by a number of overlapping phenomena which are not always directly correlated to the polymer properties, such as non-homogenous distribution of the fibers direction, entanglements and bundling [8,53]. Following Eqs. (5) and (6) it was also possible to introduce two additional parameters useful to better define the material behaviour, as sketched in Fig. 12A, and in particular:

1) the tangent line at the origin of the stress-strain curve, described by Eq. (7)

$$\sigma(\varepsilon) = E_0\varepsilon \tag{7}$$

2) and the line that best fit the linear trend of the stress-strain curve at high strain values, i.e. the tangent of the curve portion in linear region (Stage II), such as described in Eq. (8)

$$\sigma(\varepsilon) = E_{lin}\varepsilon + b \tag{8}$$

The intersection of the two straight lines from Eqs. (7) and (8) provides the onset extrapolation of the slope change, i.e. a knee which can be used to represent the switch from the highest initial slope to the linear section of the stress-strain curve. Moreover, it is possible to demonstrate that the strain at the intersection, ε_{knee}, equals 1/c, where c is the parameter evaluated based on Eq. (3) (see Supplementary Information, Fig. S4). The evaluation of ε_{knee} from the experimental curves (see Supplementary Information, Fig. S5) shows a peculiar trend of such parameter when plotted as a function of PCL fraction in the blend, as displayed in Fig. 12B. Such a figure clearly highlights that, by increasing the content of NBR in the blend, the strain value at which the knee takes place increases.

While the initial lowering of stiffness might stem from the reorganization of fibers in the network, the reduction of intersections and the breaking of such fibers already bearing a load, asymptotic tendency of the stiffness could be mainly ascribed to fibers ordering along displacement direction. In the present case, both linear and non-linear E behaviours are affected in a similar way by the NBR addition to the nanofibrous mat, denoting a relevant effect of the liquid rubber to its mechanical behaviour throughout the entire deformation range, in agreement with the assumption that a stable thermoplastic elastomeric morphology has been obtained. The transition from one type of prevailing behaviour to the other is also influenced by the fiber thickness, their prevailing alignment and the presence of weld joints. This behaviour could stem from the fact that the initial non-linear behaviour, with higher stiffness, that was attributed to deformation of the network complex system toward a more ordered one, is hampered by the presence of weld joints and plastic deformation induced by the NBR increasing content.

4. Conclusion

The ability to obtain electrospun nanofibrous mats based on homogeneous blends of liquid NBR rubber and PCL with a wide range of composition was here discussed and demonstrated. Such membranes show a single, low-temperature T_g and a surprisingly high PCL-like crystal phase content promoted by the presence of NBR.

This morphology well compares with the one of thermoplastic elastomers (TPE) and provides the membranes with excellent long-term stability (at least two years) without the need for a chemical rubber crosslinking. This morphology reflects also in a relevant mechanical performance which is improved with respect to the plain PCL nanofibers and thus shows promising properties that can be exploited in many fields, such as in composite modification. Additionally, these results were interpreted using a recently proposed phenomenological model, whose parameters are evaluated and explained taking into account nanofibers composition and morphology. While this is a preliminary model, whose terms' physical significance has still to be fully disclosed, the outstanding fitting ability validates its significance as a tool for the interpretation of nanofibrous mats mechanical behaviour.

Finally, the present formulation paves the way for implementing an easy additional cross-linking step to the present process, when in the presence of a convenient initiator system, leading to some easily obtained nanofibrous rubbery sponges, whose feature can be easily controlled.

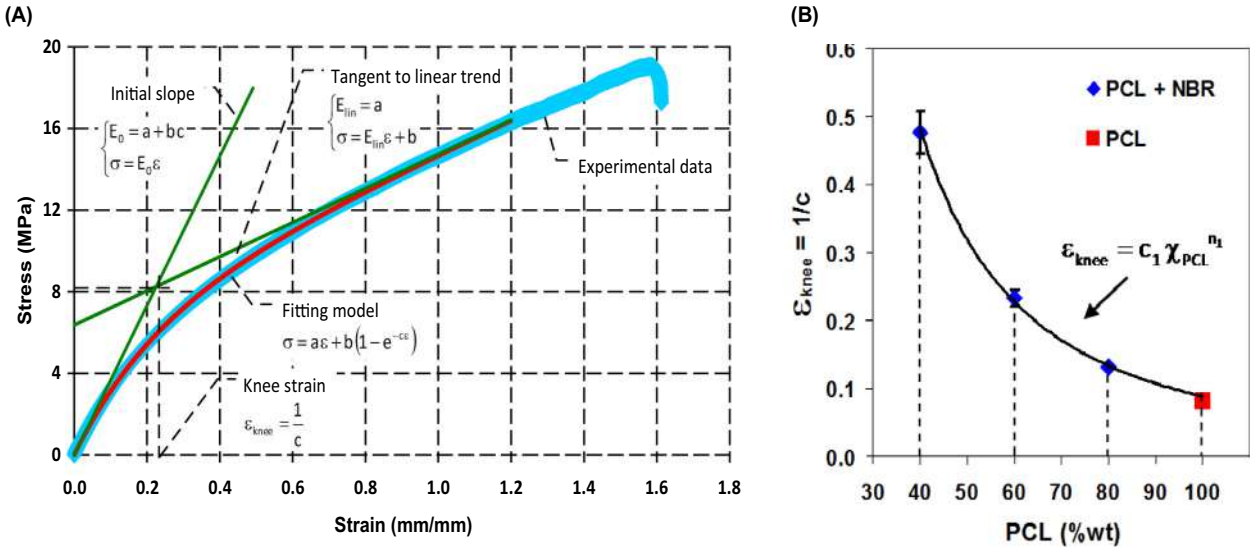

Fig. 12. A) Representation of the experimental data of the fitting model and of the two lines which describe the initial (E_0) and the linear (E_{lin}) range tangents to the curve, according to Eq. 12 and 13. B) Plot of ε_{knee} as a function of the PCL weight fraction in the blends. The interpolating function relates the ε_{knee} to the PCL weight percentage (χ_{PCL}) and the best fitting constants are $c_1 = 440$ and $n_1 = -1.85$.

Please cite this article as: E. Maccaferri, L. Mazzocchetti, T. Benelli, et al., Rubbery nanofibers by co-electrospinning of almost immiscible NBR and PCL blends, Materials and Design, https://doi.org/10.1016/j.matdes.2019.108210

Credit author statement

Conception and design of study: E. Maccaferri, L. Mazzocchetti, A. Zucchelli, L. Giorgini

Acquisition of data: E. Maccaferri, T.M. Brugo

Analysis and/or interpretation of data: E. Maccaferri, L. Mazzocchetti, T. Benelli, T.M. Brugo, A. Zucchelli, L. Giorgini

Drafting the manuscript: E. Maccaferri, L. Mazzocchetti, T. Benelli, T.M. Brugo, A. Zucchelli, L. Giorgini

Revising the manuscript critically for important intellectual content: E. Maccaferri, L. Mazzocchetti, T. Benelli, T.M. Brugo, A. Zucchelli, L. Giorgini

Approval of the version of the manuscript to be published (the names of all authors must be listed): E. Maccaferri, L. Mazzocchetti, T. Benelli, T.M. Brugo, A. Zucchelli, L. Giorgini

Acknowledgments

Authors wish to acknowledge the project "TEAM SAVE – E91B18000460007" (PG/2018/632196) of framework POR FESR 2014-2020 funded by Regione Emilia-Romagna with DGR 986/2018 for financial support.

Appendix A. Supplementary data

Additional details regarding: detailed composition of the starting solutions (Table S1), SEM micrographs of aged nanofibers (Fig. S1), in depth calculation of miscibility parameters based on Hoftyzer and van Krevelen theory (Paragraph SI1), as well as Nishi-Wang equation for the evaluation of melting point depression of miscible blends (Paragraph SI2), density evaluation of the blends (Table S4) together with material supporting the detailed application of the data fitting model (Paragraph SI3) are reported on line. Supplementary data to this article can be found online at doi: https://doi.org/10.1016/j.matdes.2019.108210.

References

[1] D. Papkov, N. Delpouve, L. Delbreilh, S. Araujo, T. Stockdale, S. Mamedov, K. Maleckis, Y. Zou, M.N. Andalib, E. Dargent, et al., Quantifying polymer chain orientation in strong and tough nanofibers with low crystallinity: toward next generation nanostructured superfibers, ACS Nano 13 (5) (2019) 4893–4927.

[2] S. Wu, P. Liu, Y. Zhang, H. Zhang, X. Qin, Flexible and conductive nanofiber-structured single yarn sensor for smart wearable devices, Sensors Actuators B Chem. 252 (2017) 697–705.

[3] A.C.C. Bortolassi, S. Nagarajan, B. de Araújo Lima, V.G. Guerra, M.L. Aguiar, V. Huon, L. Soussan, D. Cornu, P. Miele, M. Bechelany, Efficient nanoparticles removal and bactericidal action of electrospun nanofibers membranes for air filtration, Mater. Sci. Eng. C 102 (2019) 718–729.

[4] A. Sensini, C. Gualandi, M.L. Focarete, J. Belcari, A. Zucchelli, L. Boyle, G.C. Reilly, A.P. Kao, G. Tozzi, L. Cristofolini, Multiscale hierarchical bioresorbable scaffolds for the regeneration of tendons and ligaments, Biofabrication 11 (3) (2019).

[5] D. Fabiani, F. Grolli, M. Speranza, S.V. Suraci, T.M. Brugo, A. Zucchelli, E. Maccaferri, Piezoelectric nanofibers for integration in multifunctional materials, 2018 IEEE Conf. Electr. Insul. Dielectr. Phenom 2018, pp. 14–17.

[6] R. Palazzetti, A. Zucchelli, Electrospun nanofibers as reinforcement for composite laminates materials – a review, Compos. Struct. 182 (2017) 711–727.

[7] L. Sisti, J. Belcari, L. Mazzocchetti, G. Totaro, M. Vannini, L. Giorgini, A. Zucchelli, A. Celli, Multicomponent reinforcing system for poly(butylene succinate): composites containing poly(l-lactide) electrospun mats loaded with graphene, Polym. Test. 50 (2016) 283–291.

[8] L. Mazzocchetti, T. Benelli, E. Maccaferri, S. Merighi, J. Belcari, A. Zucchelli, L. Giorgini, Poly-m-aramid electrospun nanofibrous mats as high-performance flame retardants for carbon Fiber reinforced composites, Compos. Part B Eng. 145 (2018) 252–260.

[9] C.W. Wise, W.D. Cook, A.A. Goodwin, CTBN rubber phase precipitation in model epoxy resins, Polymer (Guildf) 41 (2000) 4625–4633.

[10] C.K. Riew, A.R. Siebert, R.W. Smith, M. Fernando, A.J. Kinloch, Toughened epoxy resins: Preformed particles as Tougheners for adhesives and matrices, *Toughened Plastics II*; Advances in Chemistry, 252, American Chemical Society 1996, pp. 33–44.

[11] X. Wang, H. Nie, D. Liu, A. He, Retardation of cold flow in immiscible rubber blends by tailoring their microstructures, Polym. Int. 66 (11) (2017) 1473–1479.

[12] S.S. Choi, J.P. Hong, Y.S. Seo, S.M. Chung, C. Nah, Fabrication and characterization of electrospun polybutadiene fibers crosslinked by UV irradiation, J. Appl. Polym. Sci. 101 (4) (2006) 2333–2337.

[13] M. Tian, Q. Hu, H. Wu, L. Zhang, H. Fong, L. Zhang, Formation and morphological stability of polybutadiene rubber fibers prepared through combination of electrospinning and in-situ photo-crosslinking, Mater. Lett. 65 (19–20) (2011) 3076–3079.

[14] A. Vitale, G. Massaglia, A. Chiodoni, R. Bongiovanni, C.F. Pirri, M. Quaglio, Tuning porosity and functionality of electrospun rubber nanofiber mats by photo-crosslinking, ACS Appl. Mater. Interfaces 11 (27) (2019) 24544–24551.

[15] X. Zhang, G.G. Chase, Electrospun elastic acrylonitrile butadiene copolymer fibers, Polymer (Guildf) 97 (2016) 440–448, https://doi.org/10.1016/j.polymer.2016.05.063.

[16] H. Wu, Q. Hu, L. Zhang, H. Fong, M. Tian, Electrospun composite nanofibers of polybutadiene rubber containing uniformly distributed ag nanoparticles, Mater. Lett. 84 (2012) 5–8.

[17] X. Zhang, X. Yang, G.G. Chase, Filtration performance of electrospun acrylonitrile-butadiene elastic fiber mats in solid aerosol filtration, Sep. Purif. Technol. 186 (2017) 96–105.

[18] M.W. Thielke, E.P. Bruckner, D.L. Wong, P. Theato, Thiol-Ene modification of electrospun polybutadiene fibers crosslinked by UV irradiation, Polymer (Guildf) 55 (22) (2014) 5596–5599.

[19] T.E. Kerr-Phillips, V. Woehling, R. Agniel, G.T.M. Nguyen, F. Vidal, P. Kilmartin, C. Plesse, J. Travas-Sejdic, Electrospun rubber fibre Mats with electrochemically controllable pore sizes, J. Mater. Chem. B 3 (20) (2015) 4249–4258.

[20] H.Y. Liu, H.C. Hsieh, J.Y. Chen, C.C. Shih, W.Y. Lee, Y.C. Chiang, W.C. Chen, Fabrication and application of highly stretchable conductive fiber-based electrode of epoxy/NBR electrospun fibers spray-coated with AgNW/PU composites, Macromol. Chem. Phys. 220 (4) (2019) 1–8.

[21] H. rong Nie, C. Wang, A. He, Fabrication and chemical crosslinking of electrospun trans-polyisoprene nanofiber nonwoven, Chinese J. Polym. Sci. (English Ed.) 34 (2016) 697–708.

[22] J.R. Kim, J.J. Kim, Epoxy resins toughened with surface modified epoxidized natural rubber fibers by one-step electrospinning, Materials (Basel) 10 (2017).

[23] K. Phatcharasit, W. Taweepreda, K. Boonkerd, J.K. Kim, Electrospun epoxidized natural rubber with poly(vinyl chlorside) (ENR-PVC) nanofibrous for PEMFC applications, Adv. Mater. Res. 844 (2013) 507–510.

[24] A. Aluigi, A. Varesano, C. Vineis, A. Del Rio, Electrospinning of immiscible systems: the wool keratin/polyamide-6 case study, Mater. Des. 127 (2017) 144–153.

[25] D.J. Walsh, Polymer Blends, Comprehensive Polymer Science and Supplements, Pergamon 1989, pp. 135–154.

[26] P. Tipduangta, P. Belton, L.L. Fábián, L.Y. Wang, H. Tang, M. Eddleston, S. Qi, Electrospun polymer blend nanofibers for tunable drug delivery: the role of transformative phase separation on controlling the release rate, Mol. Pharm. 13 (1) (2016) 25–39.

[27] E. Maccaferri, L. Mazzocchetti, T. Benelli, A. Zucchelli, L. Giorgini, Morphology, thermal, mechanical properties and ageing of nylon 6,6/graphene nanofibers as nano2 materials, Compos. Part B Eng. 166 (2019) 120–129.

[28] J.H. Park, G.C. Rutledge, 50th anniversary perspective: advanced polymer fibers: high performance and ultrafine, Macromolecules 50 (2017) 5627–5642.

[29] B. Gupta, A.R. Geeta; Ray, Preparation of poly(e-caprolactone)/poly(e-caprolactone-co- lactide) (PCL/PLCL) blend filament by melt spinning bhuvanesh, Polymer (Guildf) 123 (2012) 1944–1950.

[30] S. Park, J. Kim, M.-K. Lee, C. Park, H.-D. Jung, H.-E. Kim, T.-S. Jang, Fabrication of strong, bioactive vascular grafts with PCL/collagen and PCL/silica bilayers for small-diameter vascular applications, Mater. Des. 181 (2019), 108079.

[31] A. Sensini, L. Cristofolini, Biofabrication of electrospun scaffolds for the regeneration of tendons and ligaments, Materials (Basel) 11 (10) (2018) 1–43.

[32] A. Doergens, J.A. Roether, D. Dippold, A.R. Boccaccini, D.W. Schubert, Identifying key processing parameters for the electrospinning of aligned polymer nanofibers, Mater. Lett. 140 (2015) 99–102.

[33] X. Wang, H. Zhao, L.S. Turng, Q. Li, Crystalline morphology of electrospun poly(ε-caprolactone) (PCL) nanofibers, Ind. Eng. Chem. Res. 52 (13) (2013) 4939–4949.

[34] A. Cipitria, A. Skelton, T.R. Dargaville, P.D. Dalton, D.W. Hutmacher, Design, fabrication and characterization of PCL electrospun scaffolds - a review, J. Mater. Chem. 21 (26) (2011) 9419–9453.

[35] D.W. Van Krevelen, K. Te Nijenhuis, Cohesive properties and solubility, in: D.W. Van Krevelen, N. Te, K. B. T.-P. of P (Eds.), Properties of Polymers, Fourth EElsevier, Amsterdam 2009, pp. 189–227.

[36] M.T. Shaw, Preparation of blends, Polymer Blends and Mixtures, Springer Netherlands 1985, pp. 57–67.

[37] Chandler, L. A.; Collins, E. A. Multiple glass transitions in butadiene-acrylonitrile copolymers. Rubber Chem. Technol. 43, 1465–1472.

[38] H. Ono, H. Fujiwara, S. Nishimura, Nanoscale heterogeneous structure of polyacrylonitrile-co-butadiene with different molecular mobilities analyzed by spin–spin relaxation time, Polym. J. 45 (2013) 1027–1032.

[39] R. Chowdhury, M.S. Banerji, K. Shivakumar, Development of acrylonitrile-butadiene (NBR)/polyamide thermoplastic elastomeric compositions: effect of carboxylation in the NBR phase, J. Appl. Polym. Sci. 100 (2006) 1008–1012.

[40] J. Brandrup, E.H. Immergut, E.A. Grulke, Polymer Handbook, 4th ed. A Wiley-Interscience Publication; Wiley, 1999.

[41] L. Liu, S. Li, H. Garreau, M. Vert, Selective enzymatic degradations of poly(l-lactide) and poly(ε-caprolactone) blend films, Biomacromolecules 1 (2000) 350–359.

[42] Y. Suzuki, H. Duran, W. Akram, M. Steinhart, G. Floudas, H.J. Butt, Multiple nucleation events and local dynamics of poly(ε-caprolactone) (PCL) confined to nanoporous alumina, Soft Matter 9 (2013) 9189–9198.

[43] H. Bittiger, R.H. Marchessault, W.D. Niegisch, Crystal structure of poly-ε-caprolactone, Acta Crystallogr. Sect. B Struct. Crystallogr. Cryst. Chem. 26 (1970) 1923–1927.

Please cite this article as: E. Maccaferri, L. Mazzocchetti, T. Benelli, et al., Rubbery nanofibers by co-electrospinning of almost immiscible NBR and PCL blends, Materials and Design, https://doi.org/10.1016/j.matdes.2019.108210

[44] T. Nishi, T.T. Wang, Melting point depression and kinetic effects of cooling on crystallization in poly(vinylidene fluoride)-poly(methyl methacrylate) mixtures, Macromolecules 8 (1975) 909–915.
[45] J.D. Hoffman, J.J. Weeks, Melting process and the equilibrium melting temperature of polychlorotrifluoroethylene, J. Res. Natl. Bur. Stand. Sect. A Phys. Chem. 66A (1962) 13–28.
[46] G. Holden, Thermoplastic Elastomers and Their Applications, 2000.
[47] N.P. Cheremisinoff, Condensed Encyclopedia of Polymer Engineering Terms, 2001.
[48] A. Ridruejo, C. González, J. Llorca, Micromechanisms of deformation and fracture of polypropylene nonwoven fabrics, Int. J. Solids Struct. 48 (2011) 153–162.
[49] S. Sinha-Ray, A.L. Yarin, B. Pourdeyhimi, Meltblown fiber mats and their tensile strength, Polymer (Guildf) 55 (2014) 4241–4247.
[50] K. Molnar, L.M. Vas, T. Czigany, Determination of tensile strength of electrospun single nanofibers through modeling tensile behavior of the nanofibrous mat, Compos. Part B Eng. 43 (2012) 15–21.
[51] D. Papkov, Y. Zou, M.N. Andalib, A. Goponenko, S.Z.D. Cheng, Y.A. Dzenis, Simultaneously strong and tough ultrafine continuous nanofibers, ACS Nano 7 (4) (2013) 3324–3331.
[52] A. Baji, Y.W. Mai, S.C. Wong, Effect of fiber diameter on the deformation behavior of self-assembled carbon nanotube reinforced electrospun polyamide 6,6 fibers, Mater. Sci. Eng. A 528 (2011) 6565–6572.
[53] S. Backer, D.R. Petterson, Some principles of nonwoven fabrics, Text. Res. J. 30 (9) (1960) 704–711.

Please cite this article as: E. Maccaferri, L. Mazzocchetti, T. Benelli, et al., Rubbery nanofibers by co-electrospinning of almost immiscible NBR and PCL blends, Materials and Design, https://doi.org/10.1016/j.matdes.2019.108210